The EVA code; Macroscopic modeling of radio emission from air showers based on full MC simulations including a realistic index of refraction

Krijn D. de Vries*, Olaf Scholten* and Klaus Werner†

*Kernfysisch Versneller Instituut, University of Groningen, 9747 AA Groningen, The Netherlands
†SUBATECH, Université de Nantes - IN2P3/CNRS - EMN, Nantes, France

Abstract. A comprehensive overview of the newly developed EVA-code is given. To take into account Cherenkov effects and include realistic showers in combination with shower-to-shower fluctuations we have developed the EVA code (Electric fields, using a Variable index of refraction in Air shower simulations code). The EVA-code is based on histograms obtained from a full Monte-Carlo CONEX simulation to calculate radio emission from cosmic-ray-induced air showers. The EVA-code makes use of the finite dimensions of the particle distributions to overcome the divergences in the fields due to Cherenkov effects without making any approximations.

Keywords: Radio emission, Cosmic ray air showers, Shower simulations, Index of refraction, Geomagnetic Cherenkov radiation
PACS: 95.30.Gv, 95.55.Vj, 95.85.Ry, 96.50.S-

1. INTRODUCTION

The radio detection technique for ultra-high-energy-cosmic-ray induced air showers has come to a flight in the last few years. Succesfull measurements of radio emission from air showers at the CODALEMA [1, 2] and LOPES [3, 4] set-ups lead to the construction of larger arrays of radio antennas at the Pierre Auger Observatory [5] and LOFAR [6]. Along with the progress on the experimental side came a better theoretical understanding. Where up to 2008 microscopic models in time domain like REAS [7] differed both in pulse height as well as pulse shape from the macroscopic models in time domain like MGMR [8] these differences were recently resolved [9]. At this point the models predict similar pulse shapes and the pulse height differers from 10% at large distances from the shower axis to a factor of 2-3 close to the shower axis. Furthermore, the two main emission mechanisms were established. There is the geomagnetic emission mechanism due to the deflection of charged leptons in the air shower front, and the emission due to a net excess charge in the air shower front that comes from the knock out of electrons from ambient air molecules. Up to recently all radio-emission calculations were done for an index of refraction equal to unity. Even though in air the deviation from unity is small $O(10^{-4})$, in [10] it was already shown that this deviation leads to Cherenkov effects in the emitted radio signal at distances up to 200 meters from the shower axis. In this article we discuss the EVA code [11, 12], which performs a macroscopic calculation of the radio emission from air showers. The charge and current distrubitions are directly obtained from CONEX [13, 14] Monte-Carlo simulations.

2. THE MODEL

The EVA model has its basis at the Liénard Wiechert potentials from classical electrodynamics [15]. These are given by,

$$A^{\beta}_{PL}(t,\vec{x}-\vec{\xi}(t')) = \frac{\mu_0}{4\pi}\frac{J^{\beta}_{PL}}{|\tilde{R}V|}\Big|_{t=t'}. \qquad (1)$$

The vector potential is based on the point-like four current given by,

$$J^{\beta}_{PL}(t',\vec{x}) = J^{\beta}(t')\delta^3(\vec{x}-\vec{\xi}(t')), \qquad (2)$$

and should be evaluated at the negative retarded emission time t'. The four-distance $\tilde{R}$ is defined by $\tilde{R}^0 \equiv L \equiv c(t-t')$ where L is the optical path length from the emission point to the observer and t denotes the observer time. The vector component is defined by $\tilde{R}^i = -L\partial L/\partial \xi^i$. Defining $\vec{\xi}(t') = -ct'\vec{e}_{x||}$, where $\vec{e}_{x||}$ is the unit vector pointing along the shower axis. The velocity of the shower is given by $V = c^{-1}d\xi/dt'$. To account for the finite dimensions of the shower front in the emission, we use the weight function $w(r,h)$, where r is the radial distance from the shower axis, and h the longitudinal distance behind the shower front. The shower front is defined as a fictitious point moving with the speed of light along the shower axis. To take into account for the finite dimensions of the shower front we make the convolution between the weight function and the point-like vector po-

tential. The final vector potential thus becomes,

$$A^{\mu}_{w}(t,\vec{x}) = \int d^2r \int dh \; w(\vec{r},h) A^{\mu}_{PL}(t,\vec{x}-\vec{\xi}), \quad (3)$$

The electric fields are now obtained through the standard relations $E^i = c\left(\frac{\partial A^0}{\partial x^i} - \frac{\partial A^i}{\partial ct}\right)$. Nevertheless, these derivatives have to be taken with care. For a realistic index of refraction in air the denominator in Eq. 1 can become singular leading to Cherenkov effects and we cannot simply exchange derivation and integration. The index of refraction is modeled following the law of Gladstone and Dale given by,

$$n_{\mathrm{GD}} = 1 + 0.226 \frac{\mathrm{g}}{\mathrm{cm}^2}\rho(h), \quad (4)$$

where $\rho(h)$ is the air density at a height h above sea level. To solve for the singularities due to Cherenkov effect a coordinate transformation is done defining $\vec{\eta}^{\perp} = \vec{x}^{\perp} + \vec{r}$ and $\lambda = h_k - h$. Where h_k is the critical value for h where the denominator $\tilde{R}V(h_k) = 0$. By doing this we shift the derivatives acting on the denominator to the weight function, and the singularity appears at the lower limit of the integral (for details please consult the derivation in appendix A of [12]). The final expression for the electric field is now given by,

$$\begin{aligned} E^{||} &= -c \int d^2\eta^{\perp} \int_0^{h_k} d\lambda \left\{ w' A^0_{PL} - \beta w' A^{||} + w \dot{A}^{||}_{PL} \right\} \\ E^{\perp i} &= c \int d^2\eta^{\perp} \int_0^{h_k} d\lambda \left\{ w^i A^0_{PL} + \beta w' A^{\perp i}_{PL} - \beta w \dot{A}^{\perp i}_{PL} \right\}, \end{aligned} \quad (5)$$

where the dependencies of the vector potential and the weight function have been dropped. The derivatives are defined by, $\dot{A} = \partial A/\partial ct$, $w' = dw/dh$ and $w^i = dw/dr^i$. The field is separated in the component along the shower axis $E^{||}$ and transverse to the shower axis $E^{\perp i}$ with $i = 1,2$. These expression only contain square-root divergences of the vector potential which can now safely be integrated.

3. THE EVA PACKAGE

The EVA package consists out of three different parts. First there is the CX-MC-GEO simulation from which the charge and current distributions in the shower front are obtained in histograms. CX-MC-GEO is based on the full Monte-Carlo mode of the CONEX air shower simulation program. The second part is the FITMC package which makes fits to the histograms as obtained by CX-MC-GEO. This is done to obtain smooth analytic functions of the charge and current distrubtions. These analytic expressions are used in the third part of the EVA package which is the EVA electric field calculation that calculates the negative retarded time t' and the denominator $\tilde{R}V$ for a realistic index of refraction which are used as input to solve for the electric fields as given in Eq. 5.

3.1. CX-MC-GEO and FITMC

We will now briefly consider the first two parts of the EVA package, CX-MC-GEO and FITMC. The ingredients needed for the electric field calculation done by EVA are:

- The four-current as a function of shower time, $J^{\mu}(t')$
- The lateral particle distribution in the shower front $w_1(r)$
- The longitudinal particle distribution in the shower front $w_2(r,h)$.

A radial symmetry is assumed such that $w(\vec{r},h) = 2\pi w(r,h)$. The particle distribution in the shower front is now given by,

$$w(r,h) = w_1(r) w_2(r,h), \quad (6)$$

where the lonitudinal particle distribution in the shower front $w_2(r,h)$ is a function of the radial distance r.

3.2. The air-shower front

Coherence of the radio signal is determined by the projected length scales toward the observer. With this in mind, it is easy to imagine that for observers at a large distance from the shower axis (typically at impact parameters $s > 400$ m, depending on zenith angle) the showerfront is seen as point-like and the radio signal is determined by the total number of particles over time, the profile of the longitudinal air shower evolution. As discussed in [11], when Cherenkov effects occur, a finite part of the shower profile is seen in an instant by the observer. It follows that in this regime (typically at impact parameters $s < 200$ m, depending on zenith angle), the determining length scales are the dimensions of the air-shower front.

In Fig. 1, we plot the weight function for the lateral particle distribution in the shower front $w_1(r)$ as obtained by CX-MC-GEO. Also the fit obtained using FITMC

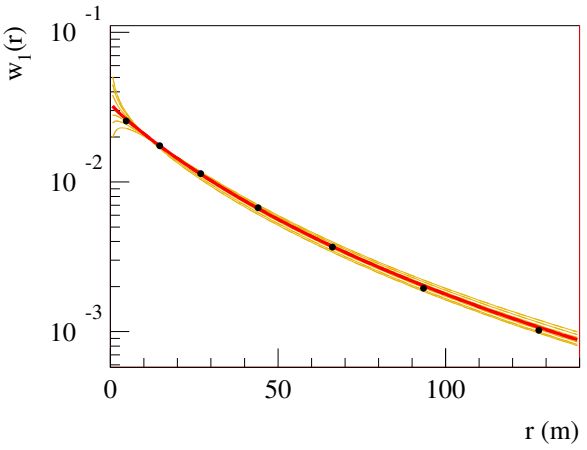

FIGURE 1. The lateral particle distribution in the shower front $w_1(r)$. The lines correspond to fits obtained with the FITMC package for different shower times. The thick (red) line correspond to the fit at the shower maximum. The dots correspond to the Monte-Carlo data obtained by CX-MC-GEO at the shower maximum.

is plotted, for the exact expressions of the fit functions we would like to refer to [12]. From Fig. 1 it is clear that most of the particles are located very close to the shower axis. In Fig. 2, we plot the longitudinal particle

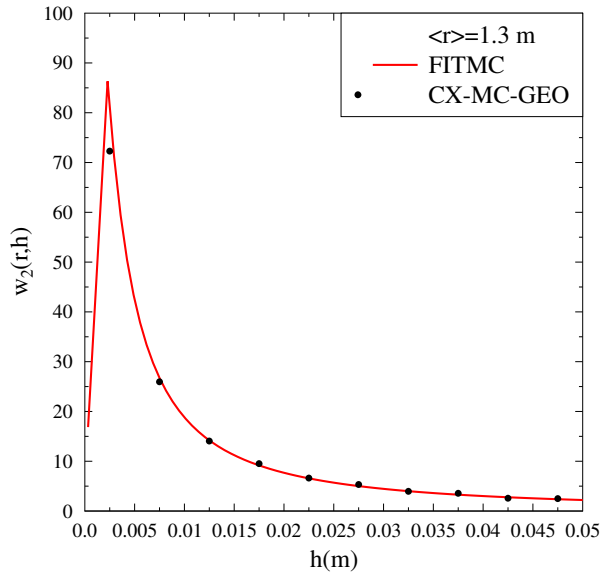

FIGURE 2. The longitudinal particle distribution at an distance $r = 1.3$ m from the shower axis, $w_2(r = 1.3\text{ m}, h)$. The full (red) line corresponds to the fit obtained by FITMC. The black dots correspond to Monte-Carlo data as obtained from the CX-MC-GEO package.

distribution at $r = 1.3$ m from the shower axis, $w_2(r = 1.3\text{ m}, h)$. It follows that at these distances the thickness of the shower front is of the order of centimeters or less and coherence can be expected in the GHz regime.

Since most of the particles are located at $< r > \approx 1$ m from the shower axis (an example of the particle distributions close to the shower axis is given in Fig. 1 of [12]), we can now approximate the projected time difference from signals emitted at opposite sides of the shower axis. For a constant index of refraction equal to its value at sea level $n = 1.0003$, the Cherenkov conditions give $\delta R \approx 2 < r > \frac{\partial R}{\partial x^{\perp}} \approx 2 < r > \sqrt{n^2\beta^2 - 1} \approx 3$ cm [16]. It is tested that this gives indeed a good estimate of the required numerical accuracy in the integration.

4. EVA VS MGMR SIMULATIONS

Both MGMR [17] and EVA are based on the macroscopic currents and particle distributions in the shower front. Where EVA is based on the currents and particle distributions directly obtained from CX-MC-GEO and FITMC, for MGMR these distributions are parameterized. Furthermore, MGMR does not take into account for Cherenkov effects. The showerfront in MGMR is parameterized by the following distribution,

$$f(h) = he^{-h/L^2}(4/L^2), \tag{7}$$

where the lateral particle distribution in the shower front is ignored and effectively taken into account for by the thickness parameter taken to be $L = 2.0$ m. In Fig. 3, the electric field is plotted as seen by an observer positioned $s = 800$ m from the shower axis for a vertical 10^{17} eV air shower. This is done for MGMR as well as EVA simulations. For the EVA simulations we plot the field for a constant index of refraction equal to unity, $n = 1$, ignoring Cherenkov effects as well as a realistic varying index of refraction following the law of Gladstone and Dale, $n = n_{GD}$. At large impact parameters we expect Cherenkov effects to diminish. Furthermore, as discussed in the previous section the determining length scale becomes the shower profile which is taken to be similar for MGMR and EVA. From Fig. 3 it follows that at $s = 800$ meters from the shower axis Cherenkov effects indeed diminish and the differences between MGMR and EVA due to the shower front are not important in this regime. In Fig. 4, the simulations are done for an observer positioned at $s = 100$ m from the shower axis. From this simulation is clear that the different treatment of the shower front in MGMR and EVA becomes more prominent. The pulse height and width between MGMR and EVA differ considerably, EVA predicts a sharper and stronger pulse than MGMR giving an indication that the width of the shower front is overestimated in MGMR.

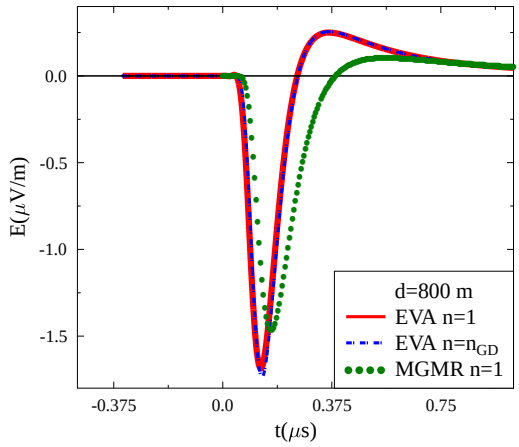

FIGURE 3. The electric field for an observer positioned at an impact parameter $s = 800$ m for a vertical 10^{17} eV air shower. The field is plotted for MGMR (green dots), and EVA with an index of refraction equal to its vacuum value of unity (solid red line) which, at these large observer distances, overlaps the field for a realistic index of refraction given by the (dashed blue line).

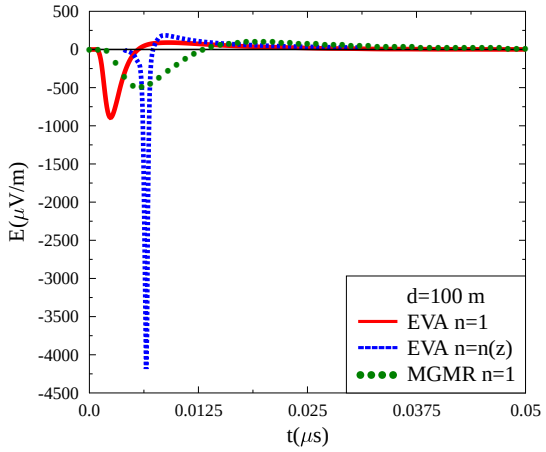

FIGURE 4. The electric field for an observer positioned at an impact parameter $s = 100$ m for a vertical 10^{17} eV air shower. The field is plotted for MGMR (green) dots, and EVA with an index of refraction equal to its vacuum value of unity full (red) line and a realistic index of refraction dashed (blue) line.

Even more prominent are the differences between the EVA simulation for an index of refraction equal to unity, $n = 1$, and a realistic index of refraction following the law of Gladstone and Dale, $n = n_{\mathrm{GD}}$. It clearly follows that Cherenkov effects are important at this distance. For a realistic index of refraction, the simulation predicts a very sharp and strong pulse clearly indicating Cherenkov effects having a response at frequencies in the GHz regime.

5. SUMMARY AND CONCLUSIONS

The EVA code consists of three different parts. First there is the CX-MC-GEO package which is a full Monte-Carlo version of the CONEX air shower simulation code. The second part is the FITMC package which is used to make fits to the histograms that are obtained from CX-MC-GEO. An example of these packages is given for the particle distributions in the shower front. It follows that close to the shower axis the particle distribution is very narrow which should give rise to GHz emission when Cherenkov effects become leading. The third part of the EVA package is the calculation of the radio emission. In the final section EVA simulations for radio emission in vacuum and for a realistic index of refraction are compared to MGMR simulations. It follows that for large observer distances, typically larger than 400 m from the shower axis, there is hardly any difference between the different simulations. At these distances the electromagnetic pulse is mainly determined by the total number of particles over time, the shower profile, and Cherenkov effects diminish. For small observer distances, typically smaller than 200 m from the shower axis, it is however shown that the different treatment of the shower front in MGMR and EVA becomes important. It also follows that Cherenkov effects are dominant in this regime and cannot be neglected. Due to these Cherenkov effects, the electromagnetic pulse becomes very sharp and strong leading to considerable power at extremely high frequencies in the GHz regime. This is a direct consequence of the narrow particle distribution in the shower front which is of the order of centimeters as discussed in the previous section. The EVA package is now publically available and can be obtained by sending an e-mail to the authors (krijndevries@gmail.com).

ACKNOWLEDGMENTS

This work is part of the research program of the 'Stichting voor Fundamenteel Onderzoek der Materie (FOM)', which is financially supported by the 'Nederlandse Organisatie voor Wetenschappelijk Onderzoek (NWO)'.

REFERENCES

1. D. Ardouin, et al., *Astropart. Phys.* **26**, 2006, pp. 341.

2. D. Ardouin and the CODALEMA Collaboration, *Astropart. Phys.* **31**, 2009, pp. 192-200.
3. H. Falcke, et al., *Nature* **435**, 2005, pp. 313.
4. W. D. Apel, et al., *Astropart. Phys.* **26**, 2006, pp. 332.
5. S. Fliescher, Pierre Auger Coll., *Nucl. Instr. and Meth. A* **662**, 2012, pp. S124-S129.
6. A. Horneffer, et al., LOFAR CR-KSP, *Nucl. Instr. and Meth. A* **617**, 2010, pp. 482.
7. T. Huege, R. Ulrich, R. Engel, *Astropart. Phys.* **27**, 2007, pp. 392-405.
8. O. Scholten, K. Werner, F. Rusydi, *Astropart. Phys.* **29**, 2008, pp. 94.
9. T. Huege, M. Ludwig, O. Scholten, and K.D. de Vries, *Nucl. Instr. and Meth. A* **662**, 2012, pp. S179-S186.
10. K. Werner, O. Scholten, *Astropart.Phys.* **29**, 2008, pp. 393.
11. K.D. de Vries, A.M. van den Berg, O. Scholten, K. Werner, *Phys. Rev. Lett.* **107**, 2011, pp. 061101.
12. K. Werner, K.D. de Vries, O. Scholten, *Astropart. Phys.* **37**, 2012, pp. 5-16.
13. G. Bossard , et al., *Phys. Rev. D* **63**, 2001, pp. 054030.
14. T. Bergmann , et al., *Astropart. Phys.* **26**, 2007, pp. 420.
15. J.D. Jackson, *Classical Electrodynamics*, Wiley, New York, 1999.
16. K.D. de Vries, O. Scholten, K. Werner, *Nucl. Instrum. Meth. A* **662**, 2012, pp. S175-S178.
17. K.D. de Vries, A.M. van den Berg, O. Scholten, K. Werner, *Astropart. Phys.* **34**, 2010, pp. 267.